

Quantum memory circuit for ion channel dynamics in the nervous system

Yu-Juan Sun¹ and Wei-Min Zhang^{1,*}

¹*Department of Physics and Center for Quantum Information Science,
National Cheng Kung University, Tainan 70101, Taiwan*

(Dated: November 20, 2024)

The opening or closing mechanism of a voltage-gated ion channel is triggered by the potential difference crossing the cell membrane in the nervous system. Based on this picture, we model the ion channel as a nanoscale two-terminal ionic tunneling junction. External time-varying voltage exerting on the two-terminal ionic tunneling junction mimics the stimulation of neurons from the outside. By deriving the quantum Langevin equation from quantum mechanics, the ion channel current is obtained by the quantum tunneling of ions controlled by the time-varying voltage. The time-varying voltage induces an effective magnetic flux which causes quantum coherence in ion tunnelings and leads to sideband effects in the ion channel current dynamics. The sideband effects in the ionic current dynamics manifest a multi-crossing hysteresis in the I-V curve, which is the memory dynamics responding to the variation of the external voltage. Such memory dynamics is defined as the active quantum memory with respect to the time-varying stimuli. We can quantitatively describe how active quantum memory is generated and changed. We find that the number of the non-zero cross points in the I-V curve hysteresis and the oscillation of the differential conductance are the characteristics for quantitatively describing the active quantum memory. We also explore the temperature dependence of the active quantum memory in such a system. The discovery of this active quantum memory characteristics provides a new understanding about the underlying mechanism of ion channel dynamics.

I. INTRODUCTION

It is widely accepted that nerve status can be demonstrated by the electrical signals carried via potential difference between the inside and outside of the cell membrane. The corresponding ion channel responses dominate the overall changes. This picture makes the nervous system look like a circuit system. There are plenty of ion channels on the neuron membrane, and each voltage-gated ion channel is usually designed as a simple circuit in electrophysiology experiments. From the electrophysiological perspective, researchers have focused on establishing a practically useful circuit theory to describe the behavior of ion channels. The prototypical example is the HH model, proposed by Hodgkin and Huxley [1] utilizing the nonlinear RC circuit, and its extensions which have successfully depicted the conductance of various ion channel clusters observed in experiments. On the other hand, looking into the protein structure of a single ion channel which can be analyzed through the X-ray crystallography, cryo-electron microscopy (cryo-EM) or high-resolution NMR techniques [2–10], the ions are transported through a single ion channel with a tiny pore. The aperture of a single ion channel is ranged from $1 \sim 15 \text{ \AA}$ [3, 11–14], while some special large conductance ion channels could reach to pore size about $40 \text{ \AA} = 4 \text{ nm}$ [15]. The nano- and subnano-scale (atomic-scale) ion channels restrict ions flow into the channels individually with the selectivity [16–18]. Under such nano- and subnano-scale and selective ability, the quantumness may play an important role in the neural signal transmission

[19–23]. However, among the works mentioned above, a general quantum biological theory has not yet been developed to explain the mechanism of neural signal transmission through ion channels.

In the literature, it has been investigated the dynamics of ion transmission utilizing the classical transport theory [24–26]. We believe that the quantumness should be taken into account from the fundamental level of quantum theory for the nano-scale ion channels and the subnanoscale (atomic) ion dynamics. A single ion channel can be analogous to a quantum molecular or atomic junction between the intracellular and extracellular ionic solutions. In this work, we propose a resonant level tunneling junction to depict such ionic junction for ion channel dynamics. The resonant level tunneling system in nanoelectronics is made with a double barrier coupled with two electrode leads and forced by external voltages. The central region between the double barriers are described as an artificial atom with quantized energy levels. Consequently, this physical process is analogous to the ions transmitting through a single ion channel (Fig. 1). The two electrode leads in the resonant level tunneling system correspond to the intracellular and extracellular ionic solutions in ion channels. In the last decade, we have developed a very general non-equilibrium time-dependent quantum transport theory [27–29, 31–33] for nanoelectronics and quantum materials. This allows us to analyze the ion transport phenomenon in the nervous system microscopically in terms of non-equilibrium quantum transport dynamics. In this non-equilibrium quantum transport dynamical theory, the ion tunnelings through the ion channel and the associated memory effects can be analyzed quantum mechanically. This could provide a new research avenue to investigate the quantum memory

* wzhang@mail.ncku.edu.tw

dynamics of ion channels in the nervous system.

If the evolution of a system is determined by the time-convolution over all its past historical evolutions, we say that the evolution of the system is a memory process. The concept of memory originally came from the learning and cognitive process of human brain. A specific memory concept related to learning and cognition is the so-called "working memory" which was first proposed by Miller, Galanter, and Pribram in 1960 [34], and has been described in many models [35–39]. Among those investigations, there are two influential models in different directions have been proposed, the multi-component memory model and the active long-term memory model. The multi-component memory model says that the working memory is dominated by the central executive and interacts with three parts: the episodic buffer, the phonological loop, and the visuospatial sketchpad [37]. The active long-term memory model more directly incorporates working memory into long-term memory (LTM) [38–41]. LTM contains the knowledge acquired in the past and significant events in our lives. These rich LTMs come from short-term memories (STMs) and are formed by repeatedly learning or suffering events that have a great impact. For example, when memorizing English vocabulary, one relies on repeated reading, writing, or using prefixes or suffixes to make our memory more profound. The existence of STM allows one to possess some data for a short period of time and conduct in-depth thinking by tracing back the LTM in the past, and then forming a new LTM. Although the architectures are different, the concepts of working memory are the same, basically for repeatedly generating memories through external influences with a phenomenological and qualitative approach. It still lacks a quantitative description of dynamical memory mechanisms based on fundamental physics principles at the molecular and atomic levels.

On the other hand, with the rapid development of quantum science and technology, in particular, quantum computing and quantum information in the last two decades, there are extensive investigations of open quantum systems with the dissipative memory (also called the non-Markovian memory) induced by the system-environment backactions. From the open quantum system point of view, the relevant system of interest interacts with surrounding environments, causing the dissipative and decoherent quantum dynamics. In particular, for many surrounding environments, especially for the structural or engineering environments, the decoherence is mainly dominated by various non-Markovian memory dynamics of quantum processes [42–45], where the memory incorporates all the backactions from environments. Each environment can be characterized uniquely by a spectral density function of the corresponding physical systems [46]. It describes in details the interactions between the system and its environment and the environmental quantum spectral structure [45].

To explore neural signal transmissions in the nervous system, ion channels embedded in the cell membrane are

treated as the systems of interest, and the intracellular and extracellular ionic solution near the ion channels are considered as the surrounding environments. To mimics the stimulation of neurons from the outside, we exerts external time-varying voltages on the intracellular and extracellular ionic solution (the two side of the ionic junction) as the outside and inside potentials of the membrane. The time-varying voltages can change significantly the original spectral density structure of the intracellular and extracellular ionic solutions. In particular, the external time-varying voltage induces effective magnetic flux phase for ion tunnelings passing through the ion channel. These effective magnetic flux-associated phases generate the quantum coherence in the ion tunneling dynamics and lead to an additional memory effect. We call this memory effect as the active quantum memory. The phenomenon of active quantum memory can be observed in the ion transmission processes. It results in a ringing transport current in the ion channel, referred to as the sideband effect [28, 47, 48]. The sideband effect manifested in the transient ionic current is the strong evidence of the circuit carrying with quantum memory and nonlinearity, demonstrated by the emergence of the multi-crossing hysteresis in the I-V curve. The emergence of the multi-crossing I-V curve hysteresis in the ion transport gives rise to a quantitative description of the active quantum memory effect in the nervous system, as it is responding to the external potential changes.

Furthermore, in the ionic tunneling junction, the quantized energy level sensitively makes the current transmittance rate vary following the changes of external potential. It is the current increasing and decreasing repeatedly that forms the sideband effect. Correspondingly, there occurs negative differential conductance which has been observed in the resonant tunneling system [49–56]. The time-dependent current was indeed investigated extensively in nanoelectronics [28, 32, 47, 48, 57, 58]. Here, in terms of open quantum system approach, we utilize the equation of motion approach to study the ion channel current and the corresponding differential conductance [31, 32]. Our goal is to quantitatively characterize the amount of active quantum memory in the ion channel current. Furthermore, the temperature dependency of the active quantum memory is also explored in this work. We believe that this formulation of active quantum memory in ion channel dynamics is homologous with the concept of working memory induced from the external stimuli in the nervous system. Also, for the practical applications, developing such a theory for quantum memory circuits should be useful in the development of neuromorphic computing technology in the future.

The neuromorphic computing is a brain-inspired computation framework different from the von Neumann architecture. It has the ability of speeding up the conventional computation, reducing the energy consumption, and making the computer flexible for learning. In the hardware aspect, memristor has been considered as a key component for neuromorphic computation. The concept

of memristor was proposed by Leon O. Chua in 1971, representing a time-dependent resistor changed with memory [59–61]. The implementation of a memristor is to use a mutator with a nonlinear passive element (a resistor, a capacitor or an inductor) to create a nonlinear I-V relation $V(t) = I(t)M(Q(t))$ with $M(Q(t)) = d\Phi(t)/dQ(t) = V(t)/I(t)$, where the charge $Q(t) = \int_{-\infty}^t I(\tau)d\tau$ and the magnetic flux $\Phi(t) = \int_{-\infty}^t V(\tau)d\tau$, and the forward and backward currents have different resistances. This property saves the status of the circuit and forms the memory. Since the difference between current and voltage is only a nonlinear multiplier, the I-V characteristics always pass the zero point ($V = 0, I = 0$). In Chua's idea, memristor is defined as the fourth basic passive element by defining an equation connecting charge and magnetic flux. However, this concept remains a subject of controversy and ongoing debate within the scientific community. It still lacks the fundamental physical principle for the necessity of introducing the fourth basic passive element in circuits. Although many investigations suggest that the memristor functions as a resistor with memory, only a limited number of studies have undertaken an in-depth investigation to unravel the fundamental nature of this memory phenomenon and delve into the physical principles [62, 63]. Hence, one of our objectives is to construct a quantum memory circuit for depicting the ion channel dynamics and investigating quantitatively the memory effect, in particular for searching the source of a memory circuit and understanding the diverse memory phenomena in greater depth.

The rest of the paper is organized as follows. In Sec. II, springing from the structure of ion channels, we introduce the two-terminal ionic quantum tunneling junction. By applying time-varying voltages on the two sides of the ion channel, the corresponding transient ion channel current is formulated in details. The ion tunnelings through the junction carry different quantum phases associated with effective magnetic fluxes which are induced by the external time-varying voltages. In Sec. III, we present analytic and numerical results under the wide-band limit of the spectral density for intracellular and extracellular ionic solution. The corresponding ion channel current displays sideband effect which results in the multi-crossing hysteresis in the I-V curve, as a quantum coherence effect representing the active quantum memory dynamics via the time-varying voltages. A critical parameter, the effective magnetic flux strength, is demonstrated for quantitatively counting the degree of the active quantum memory. Also, the amount of memory is characterized by the number of the non-zero-crossing points in the I-V curve hysteresis. The steady-state differential conductance is also analyzed for the different degree of active quantum memory. In addition, we also study the temperature dependence of the memory effect. From the structure of the I-V characteristics we obtained, we find that the concept of memristor does not exist in our quantum memory circuit. Then, we implement this theory to a realistic system. Finally, discussions and perspectives are made in

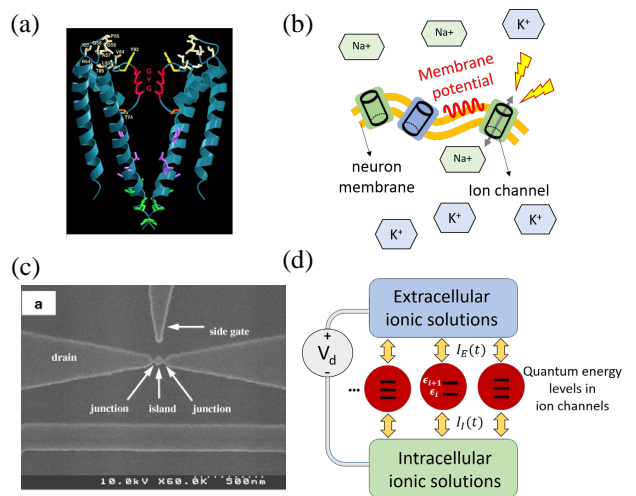


FIG. 1. (color online) Schematic plots for the connection of ion channels with the nano-scale molecular or atomic junctions. (a) The protein structure of a potassium ion channel [64]. (b) A schematic plot of an ion channel crossing the membrane. With external excitations on membrane, the ion channel opens when the membrane potential difference changes. (c) A single electron transistor (SET) under the scanning electron micrograph [65]. (d) A schematic plot of nano-scale ionic tunneling junction with left and right ionic leads mimic the intracellular and extracellular ionic solutions, respectively. The "quantum dots" (artificial atoms) with discrete quantum levels are modeled as the quantum structure of ion channels. The time-varying membrane potential difference is taken as the bias voltage (potential difference) $V_d(t) = V_E(t) - V_I(t)$ in the corresponding modeling.

Sec. IV.

II. THE QUANTUM MEMORY THEORY FOR ION CHANNEL DYNAMICS

A. A quantum modeling for ion channels

Ion channels are embedded in the membrane connecting the intracellular and extracellular ionic solution. Figure 1(a) demonstrates the protein structure of an ion channel. A schematic plot for the picture of ion channels and ions near the membrane is given in Fig. 1(b). The cluster of ions drifting near the cell membrane forms the plasma layer covering the membrane surface. The opening of the ion channel causes the ion transport through the ion channel. The action of ions inward or outward of the membrane brings the ion transport current which is driven by the potential difference (action potential) of the membrane. To construct a quantum memory circuit for ion channels, we analogize each ion channel as a molecular or atomic tunneling junction. As an example, the single electron transistor with a quantum dot (an artificial atom) in the central island, see Fig.1(c), is an ideal realization of such an atomic tunneling junction.

By connecting two "ionic leads" (corresponding to the intracellular or extracellular ionic solutions) through the coupling with a nanoscale ion channel which has discrete energy levels, we propose the quantized protein structure of an ion channel as an ionic tunneling junction, see Fig.1(d). Thus, the simplest Hamiltonian describing the quantum transmission of ions through the ion channels can have the following form,

$$\hat{H}(t) = \sum_{ij} \epsilon_{ij} \hat{a}_{ij}^\dagger \hat{a}_{ij} + \sum_{\alpha k} \epsilon_{\alpha k}(t) \hat{c}_{\alpha k}^\dagger \hat{c}_{\alpha k} + \sum_{ij\alpha k} (V_{ij\alpha k} \hat{a}_{ij}^\dagger \hat{c}_{\alpha k} + V_{ij\alpha k}^* \hat{c}_{\alpha k}^\dagger \hat{a}_{ij}), \quad (1)$$

where the first term represents the central energy levels inside the ion channels, each ion channel can contain a few (say N) discrete energy levels $\epsilon_{ij, \{j \in N\}}$, and \hat{a}_{ij}^\dagger (\hat{a}_{ij}) are the creation (annihilation) operators of the j th energy state in the i th ion channel. The second term describes the ion Hamiltonian for the intracellular and extracellular ionic solutions denoted by $\alpha = I, E$ respectively. The operators $\hat{c}_{\alpha k}^\dagger$ ($\hat{c}_{\alpha k}$) are the creation (annihilation) operators of the k th energy state of ionic charge carriers in the ionic solution α , and $\epsilon_{\alpha k}$ is the corresponding quantum energy level (usually all the energy levels form a continuous spectrum). By defining $\epsilon_{\alpha k}(t) = \epsilon_{\alpha k} + qV_\alpha(t)$, the ionic solution energy levels can be adjusted through the external time-varying voltage (potential) $V_\alpha(t)$, where q is the charge of each ion. Note that in the neuron ion channels, the transport ions are typically the sodium and potassium ions, Na^+ and K^+ , both carry a positive charge q . The bias voltage, $V_b(t) = V_E(t) - V_I(t)$ represents the time-varying potential difference between the membrane, caused by the stimulations of neurons from the outside. The third term denotes the tunneling interaction of ions between the central sites and the ionic solutions, and $V_{i\alpha k}$ is the corresponding tunneling amplitude. Also note that Na^+ and K^+ have a half-integer spin ($s = 3/2$) so that they can be treated as fermionic particles. Thus, all the creation and annihilation operators, \hat{a}_{ij}^\dagger (\hat{a}_{ij}) and $\hat{c}_{\alpha k}^\dagger$ ($\hat{c}_{\alpha k}$), obey the anti-commutation relations and the ion occupations obey the Fermi-Dirac statistical distribution in the equilibrium state.

B. A general quantum theory for the memory dynamics in ion channels

The dynamics of ion quantum transport in the above circuit can be completely determined from the quantum Heisenberg equation of motion in the Heisenberg picture of quantum mechanics,

$$\frac{d}{dt} \hat{O}(t) = \frac{1}{i\hbar} [\hat{O}(t), \hat{H}(t)], \quad (2)$$

where $\hat{O}(t)$ is any quantum operator in the Heisenberg picture, i is the imaginary number and $\hbar = h/2\pi$ is the

Planck constant. The commutation relation in Eq. (2) is defined by $[\hat{O}(t), \hat{H}(t)] = \hat{O}(t)\hat{H}(t) - \hat{H}(t)\hat{O}(t)$. Given the Hamiltonian of Eq. (1), we obtain,

$$\frac{d\hat{a}_{ij}(t)}{dt} = -\frac{i}{\hbar} \epsilon_{ij} \hat{a}_{ij}(t) - \frac{i}{\hbar} \sum_{\alpha k} V_{ij\alpha k} \hat{c}_{\alpha k}(t), \quad (3a)$$

$$\frac{d\hat{c}_{\alpha k}(t)}{dt} = -\frac{i}{\hbar} [\epsilon_{\alpha k} + qV_\alpha(t)] \hat{c}_{\alpha k}(t) - \frac{i}{\hbar} \sum_{ij} V_{ij\alpha k}^* \hat{a}_{ij}(t). \quad (3b)$$

By formally solving Eq. (3b), we have

$$\hat{c}_{\alpha k}(t) = e^{-\frac{i}{\hbar} \int_{t_0}^t dt' [\epsilon_{\alpha k} + qV_\alpha(t')]} \hat{c}_{\alpha k}(t_0) - \frac{i}{\hbar} \sum_{ij} \int_{t_0}^t dt' V_{ij\alpha k}^* e^{-\frac{i}{\hbar} \int_{t_0}^{t'} dt'' [\epsilon_{\alpha k} + qV_\alpha(t'')]} \hat{a}_{ij}(t''). \quad (4)$$

Substituting this solution into Eq. (3a), we obtain the following time-convolution equation of motion for ions,

$$\frac{d}{dt} \hat{\mathbf{a}}(t) + \frac{i}{\hbar} \boldsymbol{\epsilon}_s \hat{\mathbf{a}}(t) + \int_{t_0}^t dt' \mathbf{g}(t, t') \hat{\mathbf{a}}(t') = \hat{\mathbf{f}}(t). \quad (5)$$

where $\hat{\mathbf{a}}(t)$ ($\hat{\mathbf{a}}^\dagger(t)$) represents the ion annihilation and creation operator matrix $\{\hat{a}_{ij}(t)\}$, and $\boldsymbol{\epsilon}_s$ is the energy level matrix $\{\epsilon_{ij}\}$ for all the ion channels crossing the membrane. Here the integral kernel is a tensor matrix with matrix element $[\mathbf{g}(t, t')]_{ij, i'j'}$. It represents the memory describing historical ionic backactions between the central ion channel region and the surrounding ionic solution. The inhomogeneous term in the right-side of the above equation, $[\hat{\mathbf{f}}(t)]_{ij}$, is the noise force arisen from the ionic solution, which affects the j th energy level in the i th ion channel,

$$[\mathbf{g}(t, t')]_{ij, i'j'} = \frac{1}{\hbar^2} \sum_{\alpha k} V_{ij\alpha k} V_{i'j'\alpha k}^* e^{-\frac{i}{\hbar} \int_{t_0}^t dt' [\epsilon_{\alpha k} + qV_\alpha(t')]}, \quad (6a)$$

$$[\hat{\mathbf{f}}(t)]_{ij} = -\frac{i}{\hbar} \sum_{\alpha k} V_{ij\alpha k} e^{-\frac{i}{\hbar} \int_{t_0}^t dt' [\epsilon_{\alpha k} + qV_\alpha(t')]} \hat{c}_{\alpha k}(t_0). \quad (6b)$$

The memory kernel of Eq. (6a) characterizes the detailed ion backactions in the ion transport, i.e. ions tunnel from the ion channel into the ionic solution at time t and then tunnel back into ion channel at time t' . The noise force of Eq. (6b) is induced by the thermal ions which initially live in the thermal-equilibrium ionic environment. The time-convolution equation of motion, i.e. Eq. (5), encapsulates all the ion backaction effect on the ion dynamics in the ion channels.

Furthermore, both the memory kernel and the noise force are changed by the external time-varying voltage $V_\alpha(t)$ exerted on ionic solutions. Based on Eq. (6), we find that the external time-varying voltage $V_\alpha(t)$ induces

an effective time-varying magnetic flux

$$\Phi_\alpha(t) \equiv \int_{t_0}^t V_\alpha(\tau) d\tau, \quad (7)$$

such that the memory kernel and the noise force can be re-expressed as

$$[\mathbf{g}(t, t')]_{ij, i' j'} = \frac{1}{\hbar^2} \sum_{\alpha k} V_{ij\alpha k}(t) V_{i' j' \alpha k}^*(t') e^{-\frac{i}{\hbar} \epsilon_{\alpha k} (t-t')}, \quad (8a)$$

$$[\hat{\mathbf{f}}(t)]_{ij} = -\frac{i}{\hbar} \sum_{\alpha k} V_{ij\alpha k}(t) e^{-\frac{i}{\hbar} \epsilon_{\alpha k} (t-t_0)} \hat{c}_{\alpha k}(t_0). \quad (8b)$$

where the time-varying ion tunneling amplitude is given by

$$V_{ij\alpha k}(t) = V_{ij\alpha k} e^{-i\phi_\alpha(t)}, \quad V_{ij\alpha k}^*(t) = [V_{ij\alpha k}(t)]^*. \quad (9)$$

This defines the voltage-gated ion tunnelings through the ion channel. Physically, the phase carried by the ion tunneling amplitude is induced by the voltage-associated magnetic flux $\Phi_\alpha(t)$ when the ions flowing from ion solution α into the ion channel,

$$\phi_\alpha(t) = 2\pi \frac{\Phi_\alpha(t)}{\Phi_0}, \quad (10)$$

and $\Phi_0 = h/q$ is the magnetic flux quanta. In other words, the external electric potential $V_\alpha(t)$ induces an effective magnetic flux $\Phi_\alpha(t)$ paralleling with the membrane axis such that when the ion tunnels into the ion channel, it carries a quantum phase from the magnetic flux. This is a general principle for charge particle passing through a magnetic field, as a consequence of the gauge symmetry in quantum mechanics [30].

On the other hand, Eq. (5) derived exactly from quantum mechanics is indeed a generalized quantum Langevin equation which usually describes the quantum stochastic dynamics in the fundamental non-equilibrium evolution for the generalized Brownian particles with memory. Because of the linearity of the equation, its general solution can be expressed as [31]

$$\hat{\mathbf{a}}(t) = \mathbf{u}(t, t_0) \hat{\mathbf{a}}(t_0) + \hat{\mathbf{F}}(t), \quad (11)$$

where $\mathbf{u}(t, t')$ is called as the generalized retarded Green function matrix in the non-equilibrium dynamics, and $\hat{\mathbf{F}}(t)$ is a noise field [28, 31, 32]. Both of them determine the ion dynamics in the ion channels through ion backactions between the central region of the ion channel and the intracellular and extracellular ionic solution. Substituting this solution into Eq. (5), we can show that the non-equilibrium Green function $\mathbf{u}(t, t')$ and the noise field $\hat{\mathbf{F}}(t)$ obey the following homogenous and inhomogenous time-convolution equations of motion,

$$\frac{d}{dt} \mathbf{u}(t, t_0) + \frac{i}{\hbar} \epsilon_s \mathbf{u}(t, t_0) + \int_{t_0}^t dt' \mathbf{g}(t, t') \mathbf{u}(t', t_0) = 0, \quad (12a)$$

$$\frac{d}{dt} \hat{\mathbf{F}}(t) + \frac{i}{\hbar} \epsilon_s \hat{\mathbf{F}}(t) + \int_{t_0}^t dt' \mathbf{g}(t, t') \hat{\mathbf{F}}(t') = \hat{\mathbf{f}}(t), \quad (12b)$$

subjected to the boundary condition $\mathbf{u}(t_0, t_0) = 1$ and $\hat{\mathbf{F}}(t_0) = 0$.

As a result of Eq. (5), the integro-differential equations of Eq. (12) are also the time-convolution equations of motion that encompass all possible memory dynamics arisen from the ion backactions and are manifested through the time-convolution integrals. Indeed, the noise field of Eq. (12b) has the analytical solution,

$$\hat{\mathbf{F}}(t) = \sum_{\alpha} \int_{t_0}^t dt' \mathbf{u}(t, t') \hat{\mathbf{f}}_{\alpha}(t'). \quad (13)$$

Without loss of generality, we take the initial state of the total system (the ion channel plus the ionic solution surrounding the membrane) as $\rho_{\text{tot}}(t_0) = \rho_s(t_0) \otimes \rho_E(t_0) \otimes \rho_I(t_0)$, where the ion channel can be initially an arbitrary state, and the ionic solution surrounding the membrane are initially in thermal equilibrium state. In the Heisenberg picture of quantum mechanics, the quantum state does not change in time, namely $\rho_{\text{tot}}(t) = \rho_{\text{tot}}(t_0) \equiv \rho_{\text{tot}}$. It is easy to show that the noise field induces the following noise correlation functions,

$$\langle \hat{\mathbf{F}}(t) \rangle \equiv \text{Tr}[\hat{\mathbf{F}}(t) \rho_{\text{tot}}] = 0, \quad (14a)$$

$$\langle \hat{\mathbf{F}}^\dagger(t') \hat{\mathbf{F}}(t) \rangle = \int_{t_0}^t d\tau \int_{t_0}^{\tau'} d\tau' \mathbf{u}(t, \tau) \tilde{\mathbf{g}}(\tau, \tau') \mathbf{u}^*(t', \tau'), \quad (14b)$$

where

$$[\tilde{\mathbf{g}}(t, t')]_{ij, i' j'} = \frac{1}{\hbar^2} \sum_{\alpha k} V_{ij\alpha k}(t) V_{i' j' \alpha k}^*(t') f_{\alpha}(\epsilon_{\alpha k}) e^{-\frac{i}{\hbar} \epsilon_{\alpha k} (t-t')}, \quad (15)$$

and $f_{\alpha}(\epsilon_{\alpha k})$ is the Fermi-Dirac distribution of the ion solution α in the initial equilibrium state. In fact, Eqs. (14)-(15) fully describes the general noise properties and the associated nonequilibrium fluctuation-dissipation relation for any open quantum system [28, 29, 31–33].

Furthermore, we can easily obtain the standard nonequilibrium Green functions for the ion channel dynamics

$$\mathbf{u}(t, t_0) = \langle \{\hat{\mathbf{a}}(t), \hat{\mathbf{a}}^\dagger(t_0)\} \rangle, \quad (16a)$$

$$\mathbf{v}(t, t') = \langle \hat{\mathbf{F}}^\dagger(t') \hat{\mathbf{F}}(t) \rangle, \quad (16b)$$

which are determined explicitly by Eq. (12a) and (14b). It takes into account the precisely dynamical processes of the ion transport in ion channels arisen from the external voltages. With these exact quantum mechanical formulation and solutions, the transient ion transport through ion channels and the corresponding memory dynamics can be microscopically investigated from the first principle of quantum mechanics.

C. Active quantum memory in a single ion channel driven by the time-varying voltages

Now, we focus on a single ion channel with a single energy level ϵ_s , the simplest ionic tunneling junction. Then the system Hamiltonian (first term) and the tunneling Hamiltonian (the third term) in Eq. (1) are reduced to

$$\hat{H}_S = \epsilon_s \hat{a}^\dagger \hat{a}, \quad (17a)$$

$$\hat{H}_T = \sum_{\alpha k} (V_{\alpha k} \hat{a}^\dagger \hat{c}_{\alpha k} + V_{\alpha k}^* \hat{c}_{\alpha k}^\dagger \hat{a}). \quad (17b)$$

Since the external voltages make the charge unbalanced, they cause the ions to flow into the region of lower charge concentration. The passage of ionic charges through the ion channel across the membrane describes the ion transport current. It is expressed by

$$I(t) = I_I(t) - I_E(t), \quad (18)$$

where $I_I(t)$ ($I_E(t)$) is the current of ions flowing from the ion channel to the intracellular (extracellular) ionic solution. It is defined as the time derivative of the total ion charges in the intracellular (extracellular) ionic solution. Explicitly, using the Heisenberg equation of motion, we have

$$\begin{aligned} I_\alpha(t) &\equiv q \left\langle \frac{d}{dt} \hat{N}_\alpha(t) \right\rangle = \frac{q}{i\hbar} \langle [\hat{N}_\alpha, \hat{H}] \rangle \\ &= \frac{iq}{\hbar} \sum_k \left[V_{\alpha k} \langle \hat{a}^\dagger(t) \hat{c}_{\alpha k}(t) \rangle - V_{\alpha k}^* \langle \hat{c}_{\alpha k}^\dagger(t) \hat{a}(t) \rangle \right], \end{aligned} \quad (19)$$

where $\alpha = I, E$ represent the intercellular and extracellular ionic solution, respectively, q is the charge carried by each ion. The notation $\langle \hat{O}(t) \rangle = \text{Tr}[\hat{O}(t)\rho_{tot}(t_0)]$ denotes the expectation value of any quantum observable $\hat{O}(t)$ in the Heisenberg picture of quantum mechanics. The initial state of the whole system is assumed to be given by the density matrix $\rho_{tot}(t_0) = \rho_s(t_0) \otimes \rho_I \otimes \rho_E$, where the ion channel can be initially in any arbitrary quantum state $\rho_s(t_0)$, and the intracellular and extracellular ionic solutions are initially in the thermal state, $\rho_\alpha = \frac{1}{Z_\alpha} e^{-\frac{1}{k_B T} \sum_k \epsilon_{\alpha k} \hat{c}_{\alpha k}^\dagger \hat{c}_{\alpha k}}$ ($\alpha = I, E$) in which k_B is the Boltzmann constant, T is the thermal temperature of ionic solution, and Z_α is the corresponding thermal partition function in statistical mechanics.

Using the solution of Eqs. (4) and (11), the ion current can be expressed by the ion dynamics of the ion channel alone, namely, all the intercellular and extracellular ionic solution degrees of freedom are solved. The result is

$$I_\alpha(t) = -2q \int_{t_0}^t dt' \text{Re} \left\{ u(t, t') \tilde{g}_\alpha(t', t) - g_\alpha(t', t) n(t, t') \right\}. \quad (20)$$

Here $u(t, t_0)$ is the retarded Green function determined by the time-convolution equation Eq. (12a) for a single

ion channel,

$$\frac{d}{dt} u(t, t_0) + \frac{i}{\hbar} \epsilon_s u(t, t_0) + \sum_\alpha \int_{t_0}^t dt' g_\alpha(t, t') u(t', t_0) = 0. \quad (21)$$

The function $n(t, t')$ in Eq. (20) describes the ionic correlation function in the ion channel which is determined from the following equation,

$$\begin{aligned} n(t, t') &\equiv \langle \hat{a}^\dagger(t') \hat{a}(t) \rangle \\ &= u^*(t', t_0) u(t, t_0) n(t_0) + v(t, t'), \end{aligned} \quad (22)$$

where $n(t_0) = \langle a^\dagger(t_0) a(t_0) \rangle$ is the initial ion occupation and $v(t, t')$ is the nonequilibrium ion correlated Green function in the single ion channel,

$$\begin{aligned} v(t, t') &\equiv \langle \hat{F}^\dagger(t') \hat{F}(t) \rangle \\ &= \sum_\alpha \int_{t_0}^t d\tau \int_{t_0}^{\tau'} d\tau' u(t, \tau) \tilde{g}_\alpha(\tau, \tau') u^*(t', \tau'). \end{aligned} \quad (23)$$

It describes the ion noise correlation and represents the nonequilibrium fluctuation-dissipation relation of ions in the ion channel.

As one can see, both Green functions $u(t, t_0)$ and $v(t, t')$ contain a time-convolution integral with the memory kernel $g(t, t')$ and $\tilde{g}(t, t')$, respectively. These two memory kernels are given by

$$\begin{aligned} g_\alpha(t, t') &= e^{-i[\phi_\alpha(t) - \phi_\alpha(t')]} \frac{1}{\hbar^2} \int_{-\infty}^{\infty} \frac{d\epsilon}{2\pi} J_\alpha(\epsilon) e^{-\frac{i}{\hbar} \epsilon(t-t')} \\ &= M_\alpha(t, t') g_\alpha^0(t, t'), \end{aligned} \quad (24a)$$

$$\begin{aligned} \tilde{g}_\alpha(t, t') &= e^{-i[\phi_\alpha(t) - \phi_\alpha(t')]} \frac{1}{\hbar^2} \int_{-\infty}^{\infty} \frac{d\epsilon}{2\pi} J_\alpha(\epsilon) f_\alpha(\epsilon) e^{-\frac{i}{\hbar} \epsilon(t-t')} \\ &= M_\alpha(t, t') \tilde{g}_\alpha^0(t, t'). \end{aligned} \quad (24b)$$

They encapsulate all the memory dynamics through the ion tunnelings between the ion channel and the ionic solution α under the variation of the external time-varying voltage $V_\alpha(t)$. In these memory kernels, $J_\alpha(\epsilon) = 2\pi \sum_k |V_{\alpha k}|^2 \delta(\epsilon_{\alpha k} - \epsilon)$ is the spectral density of ionic solution α surrounding the membrane, and $f_\alpha(\epsilon) = 1/[1 + e^{\frac{1}{k_B T}(\epsilon - \mu_\alpha)}]$ is the initial ion number distribution of the ionic solution α with μ_α being the corresponding ionic chemical potential.

In Eq. (24) we have also introduced a two-time memory function $M_\alpha(t, t')$ to characterize the memory effect induced by the time-varying external voltage $V_\alpha(t)$, which is determined by the voltage-associated flux phase difference given in the ion tunnelings:

$$M_\alpha(t, t') \equiv \exp \left\{ -\frac{i}{\hbar} \int_{t'}^t q V_\alpha(\tau) d\tau \right\} = e^{-i[\phi_\alpha(t) - \phi_\alpha(t')]}, \quad (25)$$

where $\phi_\alpha(t)$ is the effective magnetic flux phase induced by the external voltage $V_\alpha(t)$, as defined by Eq. 10. This

memory factor, i.e. $M_\alpha(t, t')$, changes the ion channel memory structure, manifests the quantum coherence effect during the ion tunneling and records the historical back actions of ion channel dynamics due to the external membrane potential difference. Therefore, we define this memory dynamics as the active quantum memory in this work. Note that $g_\alpha^0(t, t')$ and $\tilde{g}_\alpha^0(t, t')$ in Eq. (7) are the original memory kernels without the external voltage (corresponds to $V_\alpha(t) = 0$). They represent the spectral structure of the ionic solution as well as ion back reactions between the ion channel and the ionic solution, as the sources of the dissipation and fluctuation in the ion channel dynamics. Thus, the above formulation offers the simplest quantitative description of active quantum memory through the quantum memory circuit for a single ion channel.

III. QUANTITATIVE DESCRIPTION OF THE ACTIVE QUANTUM MEMORY

A. Transient ion transport current in a simple ion channel

For simplicity, we consider the spectral density of the ionic environment with a wide band limit, namely let the spectral density $J_\alpha(\epsilon) = \Gamma_\alpha$, where Γ_α is simply an energy-independent damping (dissipating) constant. A constant spectral density represents the ion tunnelings from the ionic solution to the ion channel having equal probability for all different energy levels in ionic solution. In other words, the background energy spectra of the ionic solution have a very flat distribution. Under such a simplification, $g_\alpha^0(t, t') = \frac{\Gamma_\alpha}{2\hbar}\delta(t - t')$ so that the ionic environment itself do not generate non-Markovian memory dynamics. The dissipation dynamics induced by the ionic environment becomes a pure damping process. Meantime, the active quantum memory factor $M_\alpha(t, t')$ also makes no effect to the dissipation dynamics. This can be seen from the memory kernel in Eq. (21), $g_\alpha(t, t') = M_\alpha(t, t')\frac{\Gamma_\alpha}{2\hbar}\delta(t - t') = \frac{\Gamma_\alpha}{2\hbar}\delta(t - t')$. Thus, the active quantum memory is fully manifested through the ion noise correlation, in terms of the ionic transport current passing through the ion channel.

Explicitly, the solution of dissipation Green function $u(t, t')$ is simply given by

$$u(t, t') = \exp\left\{-\frac{1}{\hbar}(i\epsilon_s + \Gamma_+)(t - t')\right\}, \quad (26)$$

which describes only a memoryless Markov damping ion dynamics in the ion channel without involving memory induced from the external voltage, due to the use of the constant spectral density. In the solution of Eq. (26), we have introduced the composed cross-membrane energy damping constants $\Gamma_\pm \equiv \frac{1}{2}(\Gamma_I \pm \Gamma_E)$. While, the ionic transport current determined by Eq. (20) can be reduced

to,

$$\begin{aligned} I(t) &= I_I(t) - I_E(t) \\ &= 2q\left\{\text{Re}\left[\frac{\Gamma_-}{\hbar}n(t, t) - \int_{t_0}^t dt' u(t, t')\tilde{g}_-(t', t)\right]\right\}. \end{aligned} \quad (27)$$

Here the composed memory kernels $\tilde{g}_\pm(t, \tau')$ are defined as follows

$$\tilde{g}_\pm(t, t') \equiv \tilde{g}_I(t, t') \pm \tilde{g}_E(t, t'). \quad (28)$$

Obviously, the active quantum memory factors $M_I(t, t')$ and $M_E(t, t')$ directly changes the ion dynamics in the ion channel and then dominates the memory dynamics in the ion transport, in responding to the external time-varying voltages exerting on the ion channel.

Without loss of generality, we let the initial ion charges inside of the ion channel is zero, $n(t_0) = 0$. Then, total ion particle number inside the ion channel is given by

$$\begin{aligned} n(t, t) &= \frac{1}{\hbar^2}\int\frac{d\epsilon}{2\pi}\int_{t_0}^t d\tau\int_{t_0}^t d\tau'\left[\Gamma_I f_I(\epsilon)M_I(\tau, \tau')\right. \\ &\quad \left. + \Gamma_E f_E(\epsilon)M_E(\tau, \tau')\right]e^{\frac{i}{\hbar}(\epsilon_s - \epsilon)(\tau - \tau')}e^{\frac{\Gamma_\pm}{\hbar}(\tau + \tau' - 2t)}. \end{aligned} \quad (29)$$

The corresponding the ionic transport current passing through the ion channel can be obtained,

$$\begin{aligned} I(t) &= I_I(t) - I_E(t) \\ &= \frac{2q}{\hbar}\text{Re}\left[\Gamma_-n(t, t) - \frac{1}{\hbar}\int\frac{d\epsilon}{2\pi}\int_{t_0}^t dt'\left[\Gamma_I f_I(\epsilon)M_I(t', t)\right.\right. \\ &\quad \left.\left. - \Gamma_E f_E(\epsilon)M_E(t', t)\right]e^{(-\frac{i}{\hbar}\epsilon_s + \frac{i}{\hbar}\epsilon - \frac{\Gamma_\pm}{\hbar})(t - t')}\right]. \end{aligned} \quad (30a)$$

The responses of the ion transport current to the external time-varying voltage describe the detailed active quantum memory dynamics in the ion channel.

B. Active quantum memory induced by a periodic oscillating bias potential

The active quantum memory factor $M_\alpha(t, t')$ defined in Eq.(25) is closely correlated with the quantum coherence in the ion channel dynamics, responding to the time-varying external voltage $V_\alpha(t)$. In order to find the general rules of the active quantum memory, we now apply symmetrically a sinusoidal varying voltage to the ion solution as the simplest signal exerting the membrane,

$$V_E(t) = V(t)/2, \quad V_I(t) = -V(t)/2, \quad (31a)$$

$$V(t) = V_0 + V_d \sin(\omega_d t). \quad (31b)$$

For simplification, let $V_0 = 0$. Then the active quantum memory factor of Eq. (25) becomes

$$M_{E,I}(t, t') = \exp\left\{\pm i\frac{2\pi\Phi_M}{\Phi_0}[\cos\omega_d t - \cos\omega_d t']\right\}. \quad (32)$$

where $\Phi_M = V_d/2\omega_d$ is the amplitude of the oscillating magnetic flux and $\Phi_0 = q/h$ is the magnetic flux quanta, as we mentioned before. The minus and plus signs represent respectively the external voltage $V_{E,I}(t)$ exerting on the intracellular and extracellular ionic solution $\alpha = E, I$ on the membrane surface. Thus, the memory kernel defined in Eq. (28) under the wide-band limit spectral density can be expanded in terms of the Bessel function of

the first kind, $J_m(x)$, as follows,

$$\begin{aligned} \tilde{g}_{\pm}(t, t') &= \sum_{mm'} J_n(\phi_M) J_{m'}(\phi_M) (-i)^{m-m'} \\ &\times \frac{1}{\hbar^2} \int_{-\infty}^{\infty} \frac{d\epsilon}{2\pi} \left[\Gamma_I f_I(\epsilon) e^{-i(\epsilon/\hbar - m\omega_d)t} e^{i(\epsilon/\hbar - m'\omega_d)t'} \right. \\ &\quad \left. \pm (-1)^{n-n'} \Gamma_E f_E(\epsilon) e^{-i(\epsilon/\hbar + m\omega_d)t} e^{i(\epsilon/\hbar + m'\omega_d)t'} \right], \end{aligned} \quad (33)$$

where

$$\phi_M = 2\pi \frac{\Phi_M}{\Phi_0} = \frac{V_d}{2\omega_d} \frac{q}{\hbar} \quad (34)$$

denotes the flux phase strength associated with the active driving voltage or equivalently the effective driving magnetic flux.

After specifying the structure of the quantum memory kernel $\tilde{g}_{\pm}(t, t')$, the ion occupation number in the ion channel at arbitrary time t can be found

$$\begin{aligned} n(t, t) &= \sum_{mm'} J_m(\phi_M) J_{m'}(\phi_M) (-i)^{m-m'} \int_{-\infty}^{\infty} \frac{d\epsilon}{2\pi} \left[\Gamma_I f_I(\epsilon) \frac{(e^{-i(\frac{\epsilon}{\hbar} - m\omega_d)t} - e^{-i(\frac{\epsilon_s}{\hbar} + \frac{\Gamma_{\pm}}{\hbar})t})(e^{i(\frac{\epsilon}{\hbar} - m'\omega_d)t} - e^{i(\frac{\epsilon_s}{\hbar} - \frac{\Gamma_{\pm}}{\hbar})t})}{(\epsilon - \epsilon_s - m\hbar\omega_d)(\epsilon - \epsilon_s - m'\hbar\omega_d) + i\Gamma_+ \hbar\omega_d(m - m') + \Gamma_+^2} \right. \\ &\quad \left. + (-1)^{m-n'} \Gamma_E f_E(\epsilon) \frac{(e^{-i(\frac{\epsilon}{\hbar} + m\omega_d)t} - e^{-i(\frac{\epsilon_s}{\hbar} + \frac{\Gamma_{\pm}}{\hbar})t})(e^{i(\frac{\epsilon}{\hbar} + m'\omega_d)t} - e^{i(\frac{\epsilon_s}{\hbar} - \frac{\Gamma_{\pm}}{\hbar})t})}{(\epsilon - \epsilon_s + m\hbar\omega_d)(\epsilon - \epsilon_s + m'\hbar\omega_d) - i\Gamma_+ \hbar\omega_d(m - m') + \Gamma_+^2} \right]. \end{aligned} \quad (35)$$

Then the ion transient transport current can be calcu-

lated directly through Eq. (30a),

$$\begin{aligned} I(t) &= \frac{2q}{\hbar} \text{Re} \left\{ \Gamma_- n(t, t) - i^{m-m'} \sum_{mm'} J_m(\phi_M) J_{m'}(\phi_M) \int_{-\infty}^{\infty} \frac{d\epsilon}{2\pi} \left[(-1)^{m-m'} \Gamma_I f_I(\epsilon) \frac{e^{i\omega_d(m-m')t} - e^{[i(\frac{\epsilon}{\hbar} - m'\omega_d - \frac{\epsilon_s}{\hbar}) - \frac{\Gamma_{\pm}}{\hbar}]t}}{-i(\epsilon - m\hbar\omega_d - \epsilon_s) + \Gamma_+} \right. \right. \\ &\quad \left. \left. - \Gamma_E f_E(\epsilon) \frac{e^{-i\omega_d(m-m')t} - e^{[i(\frac{\epsilon}{\hbar} + m'\omega_d - \epsilon_s) - \Gamma_+]t}}{-i(\epsilon + m\hbar\omega_d - \epsilon_s) + \Gamma_+} \right] \right\}. \end{aligned} \quad (36)$$

In Fig. 2, we show the transient current of Eq. (36) and the I-V curve with the time-dependent bias voltages $V_d(t) = V_E(t) - V_I(t) = V(t)$ of Eq. (31b). Note that the parameter Γ represents an energy unit with arbitrary scale defined by the system-environment interacting coupling ($\Gamma = \Gamma_E + \Gamma_I$). Initially, we assume that the central region is empty with the ion occupation number $n_s(t_0) = 0$. To simplify this memory model, we also set the chemical potential of the intracellular and extracellular ionic solution is zero, $\mu_{\alpha} = 0$. Fig. 2(a) shows the

variation of current with the bias voltage changes for the relatively high frequency ($\hbar\omega_d = 3\Gamma$) and low amplitude ($qV_d = 5\Gamma$). As time passes through the second cycle of the bias voltage, the varying current becomes stable. The steady-state current remains a sinusoidal behavior similar to the applied bias voltage. Since the output current has a phase delay with respect to the bias voltage, the I-V characteristic in Fig. 2(b) shows that the I-V curve has an elliptical shape without any crossing points. This result in Fig. 2(b) indeed corresponds to a linear RLC

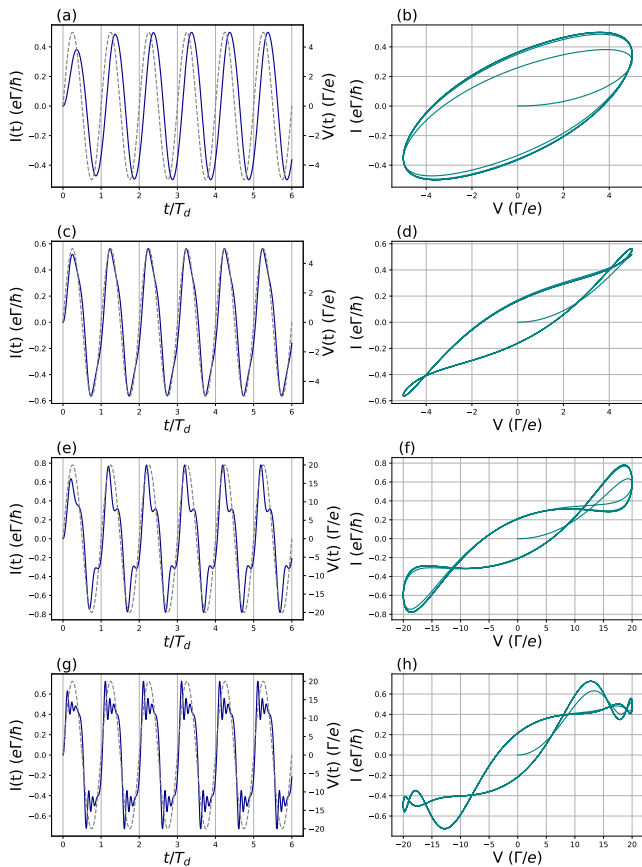


FIG. 2. (color online). The left panel is the transient ion channel current as function of the time, in responding to the time-varying bias voltage (dashed line). The right panel is the corresponding I-V curve. Non-zero crossing I-V curve hysteresis emerge for the stronger driving field amplitude V_d and lower driving frequency ω_d . The parameters are set for (a)-(b) $eV_d = 5\Gamma$, $\hbar\omega_d = 3\Gamma$; (c)-(d) $eV_d = 5\Gamma$, $\hbar\omega_d = 1\Gamma$; (e)-(f) $eV_d = 20\Gamma$, $\hbar\omega_d = 3\Gamma$; and (g)-(h) $eV_d = 20\Gamma$, $\hbar\omega_d = 1\Gamma$ (in terms of the energy unit Γ). The time unit is in the voltage period $T_d = 2\pi/\omega_d$. The temperature is $kT = 0.1\Gamma$, and the coupling to the left and right leads are $\Gamma_L = \Gamma_R = 0.5\Gamma$.

circuit.

However, by lowering the frequency from $\hbar\omega_d = 3\Gamma \rightarrow 1\Gamma$ [see Fig. 2(c)] or increasing the voltage amplitude $qV_d = 5\Gamma \rightarrow 20\Gamma$ [see Fig. 2(e)], the non-zero-crossing I-V curve hysteresis emerge, as shown in Fig. 2(d) and Fig. 2(f). By increasing further the bias voltage amplitude and decreasing the frequency, the sideband phenomenon emerges, as shown in Fig. 2(g), which results in the more complicated non-zero-crossing I-V curve hysteresis, see Fig. 2(h). Thus, we find that the emergence of sideband structure and the non-zero-crossing I-V curve hysteresis in the ion channel current is crucially related to the ratio of the high voltage amplitude V_d and low oscillating frequency ω_d , characterized by the effective magnetic flux phase strength ϕ_M . It is a direct consequence of quantum coherence given by the active quantum memory factor $M(t, t')$ of Eq. (25). A relatively high bias voltage

or low frequency increases the system's memory dynamics, while the opposite holds true for lower bias voltages or higher frequencies. This observation is consistent with the concept of "working memory" [34–39].

C. The steady-state analysis of the ion channel memory dynamics

In the ensuing paragraph, we aim to scrutinize the determinants underlying the effect of active quantum memory. As shown in Fig. (2), the ion transport current reaches the steady state after one or two periodic times, thus the steady-state time is given by $t_{st} \gtrsim 2T_d$, where $T_d = 2\pi/\omega_d$ is the period of the driving potential. In Eq. (36), the magnetic phase ϕ_M in the Bessel function characterizes the quantum coherence induced by the external bias voltage through the effective magnetic flux, see the definition given by Eq. (34). We find that this magnetic phase strength ϕ_M also serves as a descriptor of memory dynamics in ion channel, characterizing the influence of the driving bias voltage in term of the effective magnetic flux. In other words, the magnetic phase strength ϕ_M can quantify the active memory as an quantum coherence effect that we aim to discuss.

In Fig. (3), we plot the steady-state ion current through the ion channel, the I-V curve and the steady-state differential conductance with different ϕ_M values ($\phi_M = 0.1, 2, 5, 8$) by fixing the oscillating bias voltage frequency as $\hbar\omega_d = 10\Gamma$. The dark-blue lines of Fig. 3(a), (d), (g), (j) show the ion current induced by the given bias voltage, and the green lines of Fig. 3(b), (e), (h), (k) represent the formation of non-zero-crossing I-V curve hysteresis. For $\phi_M = 0.1$, the ion current has a phase delay with the input bias voltage, see Fig. 3(a), which is similar to the last example in Fig. 2(a). Its I-V curve is also similar with the linear RLC circuit, see Fig. 3(b). When ϕ_M increases, the I-V curve deforms, see Fig. 3(d) and (e) for $\phi_M = 2$. Further increasing the parameter ϕ_M , the currents show that the sideband (oscillating) dynamics, and the non-zero crossing points in the I-V curve hysteresis emerge and increase pairwise, see Fig. 3(g)-(h) and (j)-(k) for $\phi_M = 5$ and $\phi_M = 8$, respectively. With this pattern, we define the amount of active memory in terms of the number of crossing points in the I-V characteristics.

To give a further understanding of the sideband dynamics, we calculate the differential conductance

$$G(t) = dI(t)/dV(t). \quad (37)$$

The steady-state differential conductance via the change of bias voltage is presented in Fig. 3(c), (f), (i), (l) for different ϕ_M . In Fig. 3(c) ($\phi_M = 0.1$), the conductance oscillates between the plus and minus infinity, a sort of Fano resonance. The infinity conductance comes from the tuning points of in the I-V curve. However, when ϕ_M increases, and the non-zero-crossing points occur in the I-V curve hysteresis, the number of crossing points

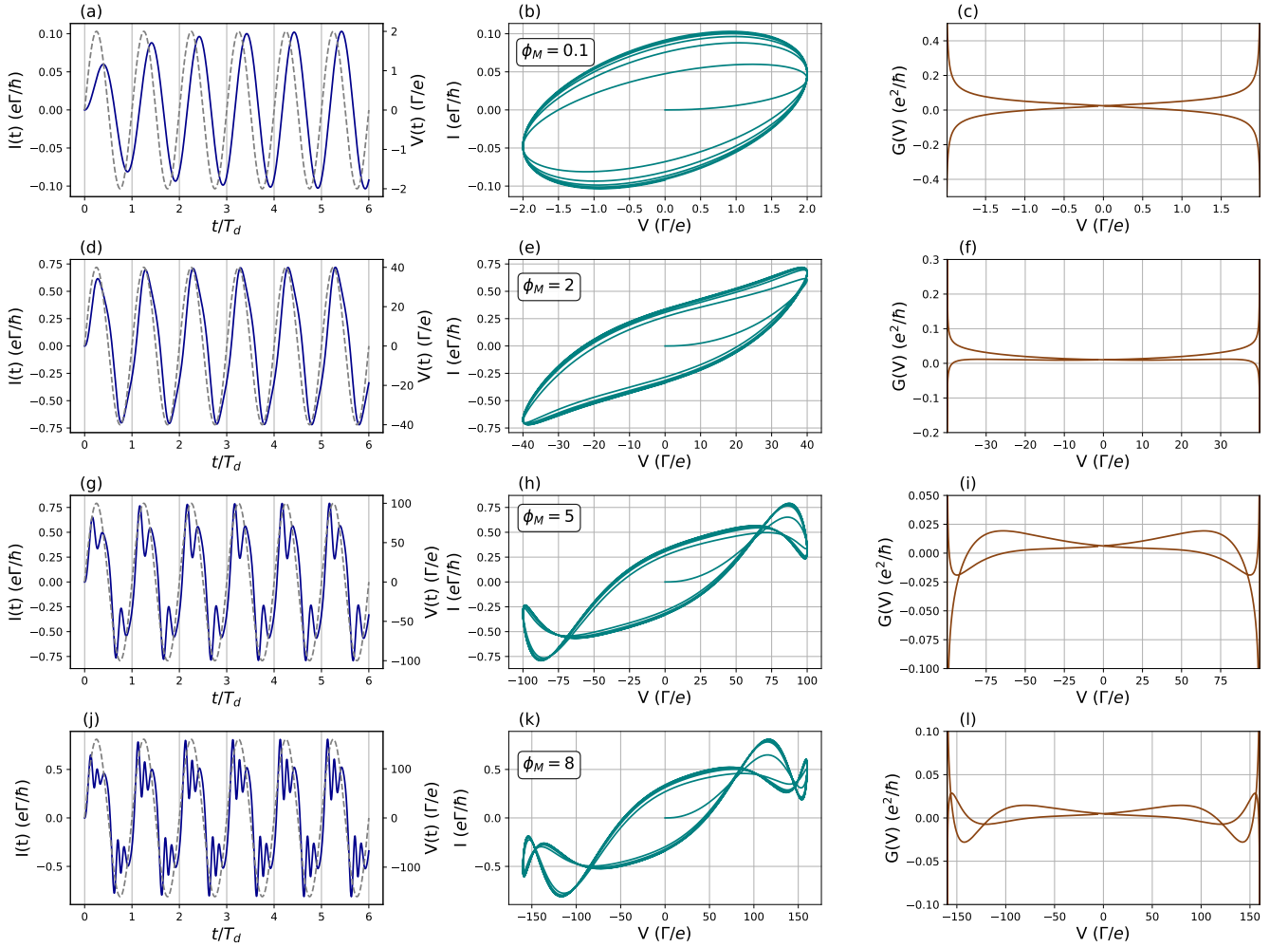


FIG. 3. (color online) The ion current (dark-blue line) changed along with the sinusoid bias voltage (dashed line) in the left panel, the corresponding I-V characteristics (green line) in the middle panel, and the steady-state differential conductance (brown line) in the right panel for different flux phase strength $\phi_M = 0.1, 2, 5, 8$ from the top plots to the bottom plots with fixed driving frequency $\hbar\omega_d = 10\Gamma$. The results show that the ion channel current reaches the steady state after two period time. The time scale here is in the unit of $T_d = 2\pi/\omega_d$. Other parameters are set as: the temperature $kT = 0.1\Gamma$, the couplings $\Gamma_L = \Gamma_R = 0.5\Gamma$, the ion channel on-site energy $\epsilon_s = 0$, and the initial ion occupation number in the ion channel $n(t_0) = 0$.

occurred in the steady-state differential conductance in a period increases similar to the non-zero-crossing points occur in the I-V curve hysteresis, see Fig. 3(i) and (l). In fact, the number of non-zero crossing points in the current-voltage (I-V) curve is equal to the number of non-zero crossing points in the differential conductance. These numbers describe quantitatively the complexity of the quantum coherence and nonlinearity in the ion transport, responding to the external time-varying voltage.

To analyze the crossing points in the I-V curves, we present a comprehensive analysis in Fig. 4. Fig. 4(a) demonstrates a contour of the current difference of forward and backward half periods,

$$D(t, \phi_M) = I(t_{st} + t, \phi_M) - I(t_{st} + 2\pi - t, \phi_M). \quad (38)$$

Here we take the steady time from the lowest bias voltage as the starting point ($t_{st} \simeq 3.5\pi/\omega_d$) to half voltage

cycle. The forward and backward currents are symmetrical at $t = t_{st} + \pi$. The cross points are located at the solution of the current difference $D(t, \phi_M) = 0$. In Fig. 4(a), the cross points represent in the white regions with the change of the magnetic phase strength ϕ_M and time. With the increasing of magnetic phase strength ϕ_M , we understand how the crossing point forms periodically and how the degree of the active quantum memory increases. Fig. 4(b) reveals a linear correlation between the number of crossing points and the magnetic phase strength ϕ_M , with an increment of two crossing points per unit increase in ϕ_M . This analysis was carried out by maintaining $\hbar\omega_d = 10\Gamma$ while varying ϕ_M from 0 to 20. The occurrence of non-zero crossing points in the I-V curve hysteresis (or equivalently in the differential conductance) indicates the presence of multiple current states at identical voltages, reflecting nonlinear

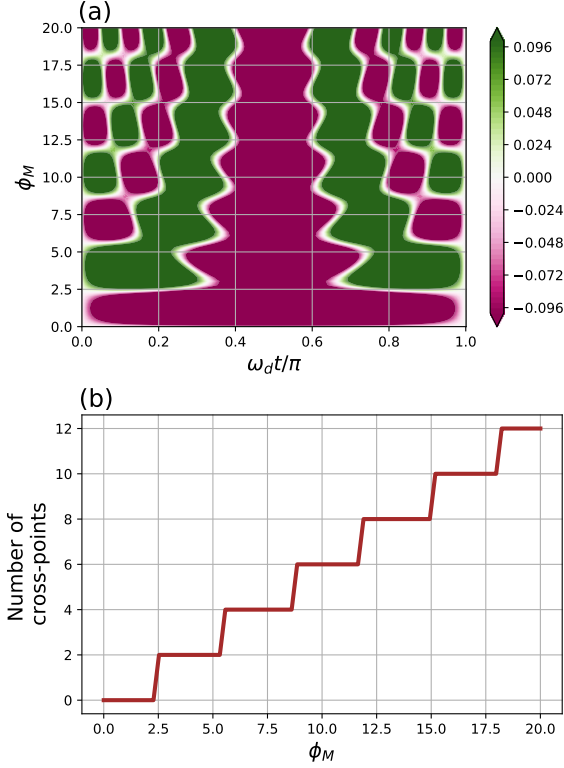


FIG. 4. (color online). The non-zero crossing point transition and the number of non-zero crossing points. (a) The contour of current difference in Eq. 38 depicts the I-V curve hysteresis change along with the different flux phase strengths ϕ_M during a cycle (a period). The solution of $D(t, \phi) = 0$ shown in the white region represents the crossing points in such time and the corresponding flux phase strength. (b) A more comprehensive diagram demonstrates the number of crossing points with different flux phase strengths ϕ_M during a cycle. The analysis was performed with ϕ_M from 0 to 20, while other parameters remained consistent with those in Fig. (3).

current responses within the ion channel. This nonlinearity, arising from the quantum coherence dynamics in ion transport, suggests that the number of crossing points may serve as a quantitative indicator of the ion channel's quantum memory capacity.

In the context of memory circuit analysis, our findings given above reveal a more fundamental memory formation compared to Chua's concept [59–61] on memristor as the fourth basic passive element in circuit theory. We show that in general the concept of memristor is not valid based on our fundamental quantum theory. In Fig. (5), we demonstrate why the concept of memristor is not valid in general, because there is no zero-crossing point in the I-V curve hysteresis. Only for the very special case, by adjusting the central energy level of the ion channel (ϵ_s), the zero-crossing points in the I-V curves may emerge. This is shown explicitly in Fig. (5), in which $\epsilon_s = 0, 5\Gamma$, and 10Γ , the crossing points in the I-V curves does not

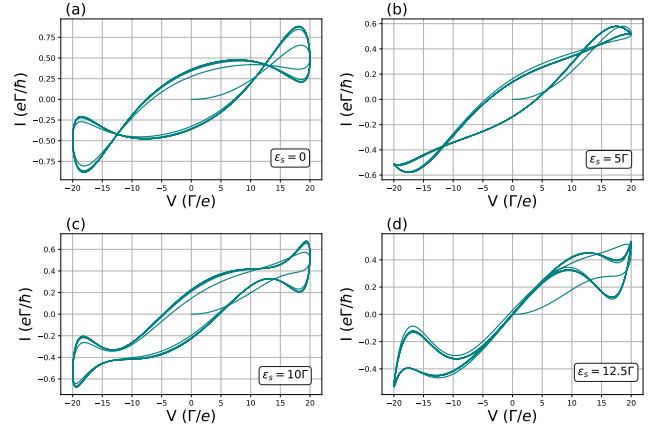


FIG. 5. (color online). The non-zero crossing I-V curve hysteresis for different on-site energy ϵ_s of the ion channel: (a) $\epsilon_s = 0$, (b) $\epsilon_s = 5\Gamma$, (c) $\epsilon_s = 10\Gamma$, (d) $\epsilon_s = 12.5\Gamma$. The bias voltage parameters $eV_d = 40\Gamma$ and $\hbar\omega_d = 5\Gamma$. The results shows that there is zero-crossing point in the I-V curve hysteresis by adjusting the system parameter, i.e. no evidence for the existence of memristor in the quantum memory circuit.

occur at the zero point ($V = 0, I = 0$). In other words, the definition of memristor $M(Q(t))$ via the I-V relation $V(t) = I(t)M(Q(t))$ cannot be satisfied in general. Only when $\epsilon_s = 12.5\Gamma$ [as shown in Fig. 5(d)], the resulting I-V nearly has a zero-crossing point, but this is not a general solution from our quantum memory theory. So we conclude that the concept of memristor as the fourth basic passive element may not exist from the fundamental physics principle. This may explain the reason why the perfect memristor has not been experimentally realized so far.

D. Temperature dependence of active quantum memory dynamics

As the last section mentions, the active quantum memory forms along with the time-varying external membrane potential, and it is described with the memory phase strength ϕ_M . However, in the high temperature, the ions in the ionic solution reach thermal equilibrium, so the system behaves more classically. The reduction of quantumness causes the active quantum memory to lose. This evidence can be shown from the two-time correlation memory kernel of Eq.(24b) by taking the temperature to be much higher than the energy scale of the ion channel $kT \gg \epsilon_s$. Then the Fermi-Dirac distribution turns into a constant number $f(\epsilon) \approx \frac{1}{2}$, and the memory kernel $\tilde{g}_\alpha^0(t-t')$ is also reduced to a delta function in time $\tilde{g}_\alpha^0(t-t') \approx \delta(t-t')$ in the wide-band limit. This makes the system become totally memoryless. Consequently, in high temperature, the contribution of the current varies as the external time-varying bias voltage, turning into a constant resistor without the quantum memory effect.

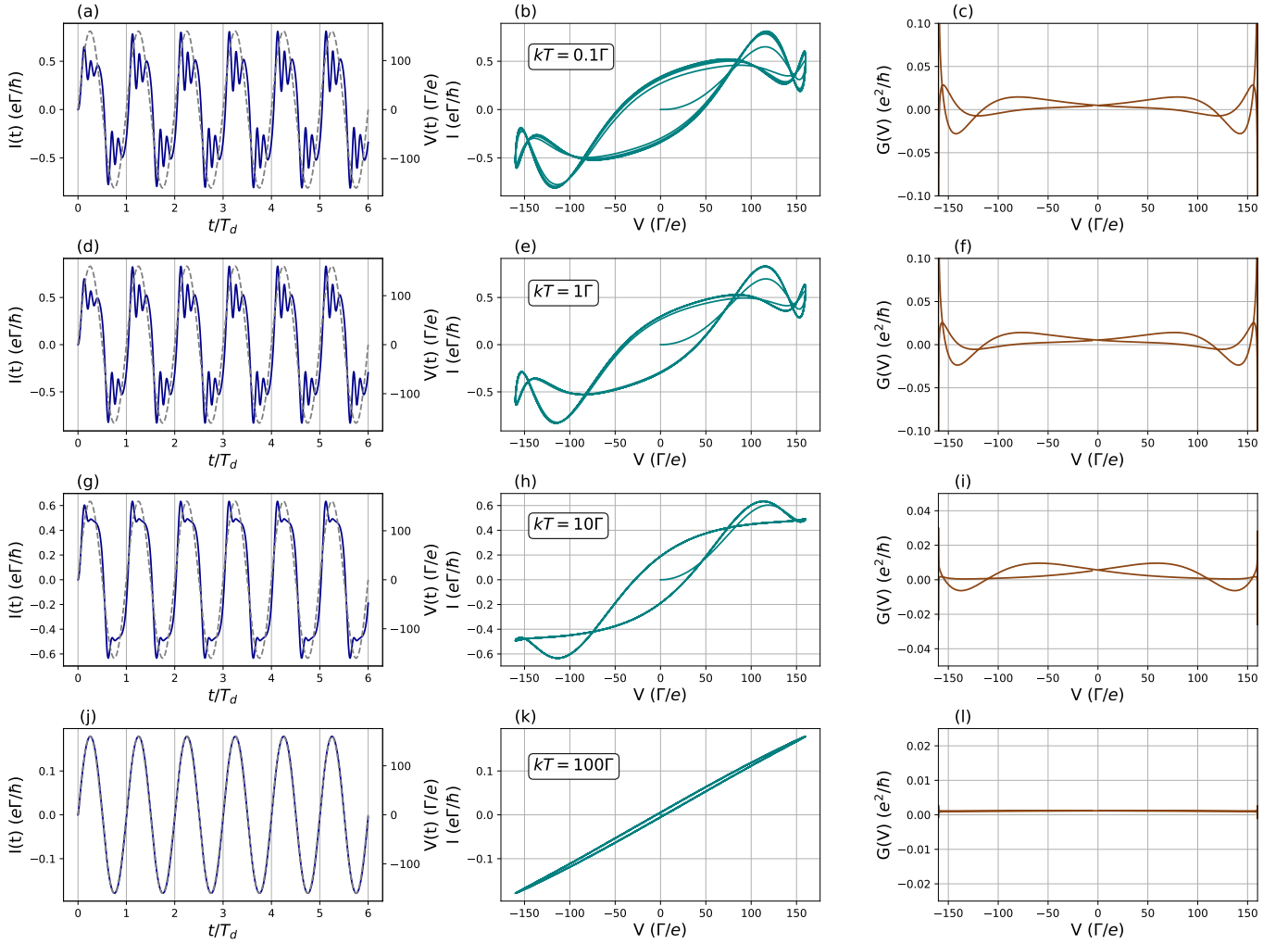


FIG. 6. (color online). The temperature dependence of the ion channel current (dark-blue line) changed along with the sinusoid bias voltage (dashed line), the I-V curve hysteresis (green line), and the steady-state differential conductance (brown line) under the oscillating bias voltage with different temperature $kT = 0.1\Gamma, 1\Gamma, 10\Gamma, 100\Gamma$ from the top panel to the bottom panel, respectively. The time scale here is in the unit of $T_d = 2\pi/\omega_d$. The flux phase strength is fixed with $\phi_M = 8$ with biasing frequency $\hbar\omega_d = 10\Gamma$, the coupling $\Gamma_L = \Gamma_R = 0.5\Gamma$, the system gate voltage $\omega_s = 0$, and the initial dot occupation number $n_0 = 0$.

To give a clear evidence of the temperature effect, we demonstrate the transient ion current, the corresponding I-V curve hysteresis, and the differential conductance by fixing $\phi_M = 8$ and changing the temperature from $kT = 0.1\Gamma, 1\Gamma, 10\Gamma$ to 100Γ , as shown in Fig. (6). The dark-blue lines in the left panel of [Fig. 6(a), (d), (g), (j)] show the ion currents driven by the same bias voltage (gray-dashed line) with the increasing temperature. The sideband effect is obvious when the system is in the low temperature ($kT = 0.1\Gamma$). In high temperature ($kT = 100\Gamma$), the sideband effect gradually disappears and the ion current becomes proportional to the input bias voltage [see Fig. 6(j)], indicating the loss of the quantum memory coherence.

The middle panel given in Fig. 6(b), (e), (h), (k) shows the I-V curve hysteresis. When the tempera-

ture increases, the cross-points reduce from 4 cross-points ($kT = 0.1\Gamma$ and 1Γ), 2 cross-points ($kT = 10\Gamma$) to 0 cross-point ($kT = 100\Gamma$). When $kT = 100\Gamma$ in Fig. 6(k), the I-V curve hysteresis becomes almost linear corresponding with a constant resistor without the memory. To give a more comprehensive description for the amount of memory in this circuit, the varying of conductance is also presented in the right panel in Fig. 6. These brown lines in Fig. 6(c), (f), (i), (l) are the differential conductance defined in Eq. (37). In the low temperature (to $kT = 0.1\Gamma$), the conductance oscillates in a period in the steady-state limit [see Fig. 6(c)]. When the temperature increases (to $kT = 100\Gamma$), the oscillation of the conductance drops and the conductance approaches to an almost constant positive value. [see Fig. 6(l)].

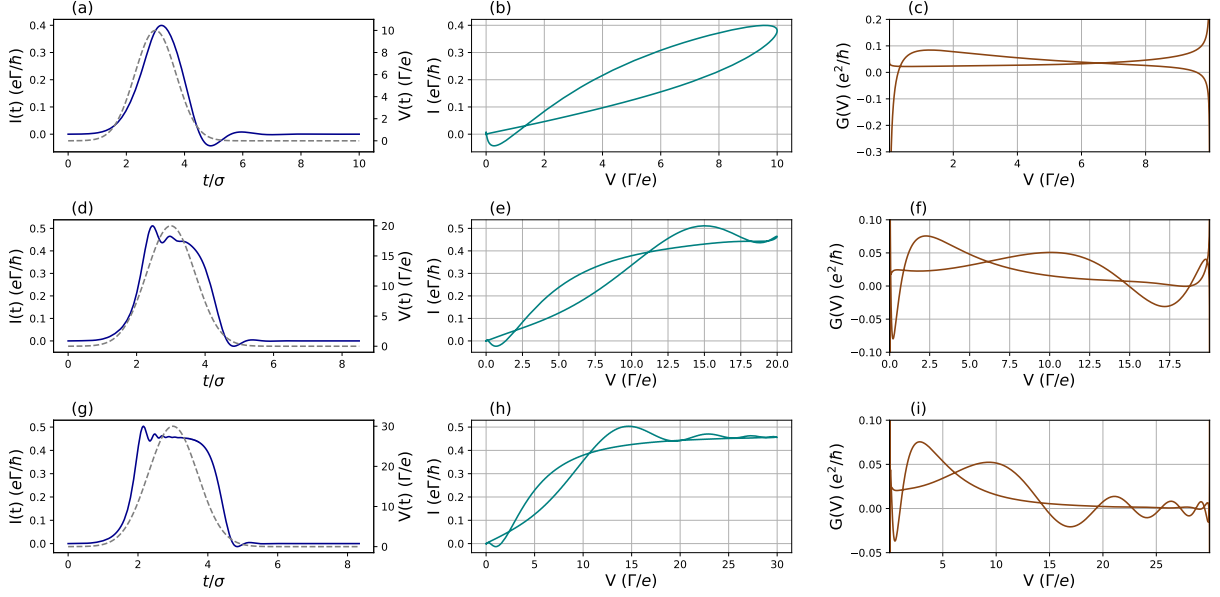


FIG. 7. (color online). A Gaussian-form bias voltage is applied to simulating a more realistic neural potential. The resulting corresponding ion current, the I-V curve hysteresis and the steady-state differential conductance are plotted with three different Gaussian parameter sets: The top panel (a)-(c) for the pulse amplitude $qV_d = 10\Gamma$ and width $\sigma = 1\hbar/\Gamma$ with the offset $\tau = 3\hbar/\Gamma$; The middle panel (d)-(f) for the amplitude $qV_d = 20\Gamma$ and width $\sigma = 2\hbar/\Gamma$ with the offset $\tau = 6\hbar/\Gamma$; The bottom panel (g)-(i) for the amplitude $qV_d = 30\Gamma$ and width $\sigma = 3\hbar/\Gamma$ with the offset $\tau = 9\hbar/\Gamma$. The system one-site energy $\epsilon_s = 3\Gamma$.

E. The ion channel current caused by an approximated membrane potential difference

After the detailed analysis of the quantum memory manifestation in the ion channel transport current via the periodic time-varying bias voltage, we now turn to consider a more realistic bias voltage in neural signal transmission. We approximate the membrane potential as a Gaussian pulse,

$$V(t) = V_d \exp \left\{ -\frac{(t - \tau)^2}{\sigma^2} \right\}. \quad (39)$$

A Gaussian pulse is quite close to the action potential in neurotransmission. Thus, the membrane potential is given by the difference of external voltages $V_\alpha(t) = \pm V(t)/2$ with $\alpha = E$ or I . The Gaussian pulse also induces the effective magnetic flux which leads to the active memory factor

$$M_{E,I}(t, t') = \exp \left\{ \pm i \frac{2\pi\Phi_M}{\Phi_0} \left[\sqrt{\pi} \operatorname{erf} \left(\frac{t - \tau}{\sigma} \right) - \sqrt{\pi} \operatorname{erf} \left(\frac{t' - \tau}{\sigma} \right) \right] \right\}. \quad (40)$$

where $\Phi_M = \frac{1}{2}V_d\sigma$ and $\operatorname{erf}(t)$ is the Gauss error function. The active memory factor controls the active quantum memory in the ion channel dynamics as we shown in the last section. It shows that the larger V_d and σ can generate stronger quantum memory dynamics.

In Fig. 7, we present the ion transport results, i.e. the transient ion current through the ion channel, the corresponding I-V curve hysteresis and the steady-state differential conductance with three different setup of the Gaussian pulse parameters. The plots in the top panel of Fig. 7 (a)-(c) corresponds to the pulse amplitude $qV_d = 10\Gamma$ and the pulse width $\sigma = 1\hbar/\Gamma$ ($\phi_M = 5$), the middle panel (d)-(f) is for amplitude $qV_d = 20\Gamma$ and the width $\sigma = 2\hbar/\Gamma$ ($\phi_M = 20$), and the bottom panel (g)-(i) is for amplitude $qV_d = 30\Gamma$ and the width $\sigma = 3\hbar/\Gamma$ ($\phi_M = 45$). For such a single potential pulse, the ion channel current demonstrates indeed the same ion transport properties as that driven by the periodic sinusoidal varying voltage. The ion current in time behaves like the action potential in the neurotransmission. The current returns to the original state after the voltage pulse. The larger effective flux phase strength results in more non-zero crossing points in I-V curve hysteresis, indicating the strong active quantum memory dynamics. This has been clearly shown in Fig. 7. When the magnetic flux phase strength ϕ_M increases, it shows the emergence and enhancement of the sideband oscillations in the ion transport current [see Fig. 7(a),(d) and (g)], the increasing number of the non-zero crossing points in I-V curve hysteresis [see Fig. 7(b), (e) and (h)], and oscillations of the differential conductance between the positive and negative values [see Fig. 7(c), (f) and (i)]. All these behaviors in the ion channel current demonstrate the active quantum memory as a quantum coherence dynamical effect, as we described in the previous subsections.

This also shows that in the nervous system, ion chan-

nels have a quantum memory effect that is induced by the external environment, and this quantum active memory effect is mainly reflected in steady-state current and conductance. Comparing this with the well-known Hodgkin-Huxley model, the HH model describes an average effect of a cluster of ion channels, the quantum coherence is wiped under the measurement of the collective result. However, our model gives a single ion channel current. The analysis suggests that the oscillating data contains not only noise signals but also quantum coherence-induced complex oscillating currents, specifically sideband structure in the ion channel currents with active quantum memory. On the other hand, the study indicates that increased environmental stimuli and extended duration of changes correlate positively with enhanced working memory performance [66–69]. According to working memory theory, sustained and gradual changes, exemplified by consistent practice, facilitate working memory formation. Therefore, we conclude that the quantum dissipative memory of the ion channel is actually the physical interpretation of working memory.

IV. DISCUSSIONS AND PRESPECTIVES

In this work, we construct a quantum memory circuit for the ion channel dynamics. We model a single ion channel as an ionic tunneling junction and study the ionic quantum transport through the ion channel. Using the quantum Langevin equation approach of open quantum system and the non-equilibrium Green's function method, we compute the ion quantum transport current passing through a single ion channel. The ion dynamics in the ion channel is determined by the time-convolution equation of motion derived for open quantum systems, and thereby provides a quantum memory description through the ion channel current. We find that the external time-varying voltage exerting on the intracellular and extracellular ionic solution near the ion channels induce an effective magnetic flux phase to the ion tunnelings and cause the quantum coherent ion transmission. We show that the effective flux phases induce quantum coherence in ion tunnelings and dominates the memory dynamics in the ion transport, in responding to the external time-varying voltage.

We define this memory dynamics as the active quantum memory. We show that the active quantum memory is associated with the sideband oscillations in the ion channel current, which provide a way how to observe the active quantum memory in experiments. We also demonstrate that the sideband oscillation structure is a significant manifestation of the quantum coherence through the effective magnetic fluxes induced by the external time-varying voltages, as the main physical origin of the active memory dynamics in the ion channel dynamics. The active quantum memory also manifests the multipole non-zero crossing points in the I-V curve hysteresis and the oscillating differential conductance. This may provide a

underlying quantum description about the connection of the active quantum memory in the ion channel dynamics with the external stimuli of the neuron membrane in the nervous system.

Throughout this study, we aim to connect a quantum memory circuit to the neurotransmission in ion channels. Regarding the study of single ion channel signals, the patch clamp method is currently the most widely used experimental method [70, 71]. Due to limitations in the signal-to-noise ratio affecting the sampling frequency, the time resolution of single-ion signal recordings remains lower, mostly at the millisecond resolution in most of electrophysiology experiments [72–75]. This may lead to measurement inaccuracies. Our analysis suggests that the oscillating data contains not only noise signals but also the quantum coherence involving in the ion tunnelings, the time resolution of measuring single ion channel current must be improved from milliseconds to microseconds and even nanoseconds. Thus, the sideband structure in the ion channel currents, the multipole non-zero crossing points in the I-V curve hysteresis and the oscillating steady-state differential conductance can be observed, as shown in this work. Based on the current nanotechnology for the nano-scale electronics with a potential difference of tens to hundred of mV (millivolts), the measured current range from a few to tens of pA (pico-ampere), it should not be difficult to make the measurement accuracy to the sub-microsecond or even nanosecond in time resolution. Of course, experiments on living cells add great difficulty.

It is well-known that ion channel dynamics is crucially important to building the science of living cells. Ion channels are especially prominent components of the nervous system. Ion channel dynamics have evolved from fundamental discoveries of cellular excitability to a complex, multidimensional field of research that intersects with molecular biology and biophysics. In this study, we only model and analyze single ion channel dynamics as a simple solvable system in quantum mechanical theory, which is still far from the complexity of real neural circuits. On the other hand, the current observations to the ion channel dynamics in experiments are mainly simulated and explained through the action potential for ion channel clusters. The advent of cryo-EM and high-resolution NMR has allowed for the detailed structural analysis of different ion channels in their functional states. Optogenetics [76, 77] and chemogenetics [78–80] techniques enable precise manipulation of ion channels in living cells. These techniques have improved our understanding of the dynamic role of ion channels in neural circuits. We hope that this work based on the underlying quantum dynamics can provide a starting point for quantum mechanics-based description of ion channel dynamics.

V. ACKNOWLEDGMENTS

This work is supported by Ministry of Science and Technology of Taiwan, Republic of China, under Contract No. MOST-111-2112-M-006-014-MY3.

-
- [1] A. L. Hodgkin, and A. F. Huxley, *A quantitative description of membrane current and its application to conduction and excitation in nerve*, J. Physiol. **117**, 500 (1952).
- [2] D. A. Doyle, J. Morais Cabral, R. A. Pfuetzner, A. Kuo, J. M. Gulbis, S. L. Cohen, B. T. Chait, and R. MacKinnon, *The Structure of the Potassium Channel: Molecular Basis of K^+ Conduction and Selectivity*, Science **280**, 69 (1998).
- [3] C. M. Armstrong, and B. Hille, *Voltage-gated ion channels and electrical excitability*, Neuron **20**, 371 (1998).
- [4] R. MacKinnon, *Potassium channels*, FEBS Lett. **555**, 62 (2003).
- [5] W. A. Catterall, *Ion channel voltage sensors: structure, function, and pathophysiology*, Neuron **67**, 915 (2010).
- [6] C. Maffeo, S. Bhattacharya, J. Yoo, D. Wells, and A. Aksimentiev, *Modeling and simulation of ion channels*, Chem. Rev. **112**, 6250 (2012).
- [7] A. K. Singh, L. L. McGoldrick, K. Saotome, and A. I. Sobolevsky, *X-ray crystallography of TRP channels*, Channels **12**, 137 (2018).
- [8] P. Phyto, X. Zhao, A. C. Templeton, W. Xu, J. K. Cheung, and Y. Su, *Understanding molecular mechanisms of biologics drug delivery and stability from NMR spectroscopy*, Adv. Drug Deliv. Rev. **174**, 1 (2021).
- [9] A. Mironenko, U. Zachariae, B. L. de Groot, and W. Kopec, *The persistent question of potassium channel permeation mechanisms*, J. Mol. Biol. **433**, 167002 (2021).
- [10] U. Günsel, and F. Hagn, *Lipid nanodiscs for high-resolution NMR studies of membrane proteins*, Chem. Rev. **122**, 9395 (2021).
- [11] O. V. Krasilnikov, R. Z. Sabirov, V. I. Ternovsky, P. G. Merzliak, and J. N. Muratkhodjaev, *A simple method for the determination of the pore radius of ion channels in planar lipid bilayer membranes*, FEMS Microbiol. Immunol. **5**, 93 (1992).
- [12] E. A. Merritt, S. Sarfaty, F. van den Akker, C. L'Hoir, J. A. Martial, and W. G. Hol, *Crystal structure of cholera toxin B-pentamer bound to receptor GM1 pentasaccharide*, Protein Sci. **3**, 166 (1994).
- [13] O. S. Smart, J. G. Neduvilil, X. Wang, B. A. Wallace, and M. S. Sansom, *HOLE: a program for the analysis of the pore dimensions of ion channel structural models*, J. Mol. Graph. **14**, 354 (1996).
- [14] G. Klesse, S. Rao, M. S. P. Sansom, and S. J. Tucker, *CHAP: A Versatile Tool for the Structural and Functional Annotation of Ion Channel Pores*, J. Mol. Biol. **431**, 3353 (2019).
- [15] C. C. Cruickshank, R. F. Minchin, A. C. Le Dain, and B. Martinac, *Estimation of the pore size of the large-conductance mechanosensitive ion channel of Escherichia coli*, Biophys. J. **73**, 1925 (1997).
- [16] D. A. Doyle, J. Morais Cabral, R. A. Pfuetzner, A. Kuo, J. M. Gulbis, S. L. Cohen, B. T. Chait, and R. MacKinnon, *The structure of the potassium channel: molecular basis of K^+ conduction and selectivity*, Science **208**, 69 (1998).
- [17] J. H. Morais-Cabral, Y. Zhou, and R. MacKinnon, *Energetic optimization of ion conduction rate by the K^+ selectivity filter*, Nature **414**, 37 (2001).
- [18] Y. Zhou, J. H. Morais-Cabral, A. Kaufman, R. MacKinnon, *Chemistry of ion coordination and hydration revealed by a K^+ channel-Fab complex at 2.0 Å resolution*, Nature **414**, 43 (2001).
- [19] S. Roy, and R. Llinás, *Relevance of quantum mechanics on some aspects of ion channel function*, C. R. Biol. **332**, 517 (2009).
- [20] J. Summhammer, V. Salari, and G. Bernroder, *A quantum-mechanical description of ion motion within the confining potentials of voltage-gated ion channels*, J. Integr. Neurosci. **11**, 123 (2012).
- [21] V. Salari, H. Naeij, and A. Shafiee, *Quantum Interference and Selectivity through Biological Ion Channels*, Sci. Rep. **7**, 41625 (2017).
- [22] T. Gonzalez-Raya, X.-H. Cheng, I. L. Egusquiza, X. Chen, M. Sanz, and E. Solano, *Quantized single-ion-channel hodgkin-huxley model for quantum neurons*, Phys. Rev. Applied **12**, 014037 (2019).
- [23] T. Gonzalez-Raya, E. Solano, and M. Sanz, *Quantized three-ion-channel neuron model for neural action potentials*, Quantum **4**, 224 (2020).
- [24] W. Fischer, J. Brickmann, and P. Lauger, *Molecular dynamics study of ion transport in transmembrane protein channels*, Biophys. Chem. **13**, 105 (1981).
- [25] K. Cooper, E. Jakobsson, and P. Wolynes, *The theory of ion transport through membrane channels*, Prog. Biophys. Mol. Biol. **46**, 51 (1985).
- [26] H.-X. Zhou, *Diffusion-Influenced Transport of Ions across a Transmembrane Channel with an Internal Binding Site*, J. Phys. Chem. Lett. **1**, 1973 (2010).
- [27] M. W. Y. Tu and W.-M. Zhang, *Non-markovian decoherence theory for a double-dot charge qubit*, Phys. Rev. B **78**, 235311 (2008).
- [28] J. Jin, M. W.-Y. Tu, W.-M. Zhang, and Y. Yan, *Non-equilibrium quantum theory for nanodevices based on the Feynman-Vernon influence functional*, New J. Phys. **12**, 083013 (2010).
- [29] C. U. Lei and W.-M. Zhang, *A quantum photonic dissipative transport theory*, Ann. Phys. **327**, 1408 (2012).
- [30] C. Cohen-Tannoudji, B. Diu, and F. Lalo e, *Quantum mechanics: Vol 1: Basic concepts, tools, and applications* 2nd ed. (Wiley-VCH, Weinheim, 2020).
- [31] P.-Y. Yang, C.-Y. Lin, and W.-M. Zhang, *Master equation approach to transient quantum transport in nanostructures incorporating initial correlations*, Phys. Rev. B **92**, 165403 (2015).
- [32] P.-Y. Yang and W.-M. Zhang, *Master equation approach to transient quantum transport in nanostructures*, Front. Phys. **12**, 127204 (2017).

- [33] C.-Z. Yao, H.-L. Lai, and W.-M. Zhang, *Quantum transport theory of hybrid superconducting systems*, Phys. Rev. B **108**, 195402 (2023).
- [34] G. A. Miller, E. Galanter, and K. H. Pribram, *Plans and the Structure of Behaviour* (Henry Holt and Co., New York, 1960).
- [35] R. C. Atkinson, R. M. Shiffrin, in *The psychology of learning and motivation: Advances in research and theory, Human memory: A proposed system and its control processes* edited by K. W. Spence and J. T. Spence (Academic Press, New York, 1968), Vol. 2, p. 89-195.
- [36] A. D. Baddeley, and G. Hitch, in *The psychology of learning and motivation: Advances in research and theory, Working memory*, edited by G. H. Bower (Academic Press, New York, 1974), Vol. 8, p. 47-89.
- [37] A. Baddeley, *The episodic buffer: a new component of working memory?*, Trends Cogn. Sci. **4**, 417 (2000).
- [38] N. Cowan, *Evolving conceptions of memory storage, selective attention, and their mutual constraints within the human information-processing system*, Psychol. Bull. **104**, 163 (1988).
- [39] N. Cowan, in *Models of Working Memory: Mechanisms of Active Maintenance and Executive Control, An Embedded-Processes Model of Working Memory*, edited by A. Miyake and P. Shah (Cambridge University Press, Cambridge, 1999), p. 62-101.
- [40] K. A. Ericsson and W. Kintsch, *Long-term working memory*, Psychol. Rev. **102**, 211 (1995).
- [41] N. Cowan, *What are the differences between long-term, short-term, and working memory?*, Prog. Brain Res. **169**, 323 (2008).
- [42] W.-M. Zhang, P.-Y. Lo, H.-N. Xiong, M. W.-Y. Tu, and F. Nori, *General Non-Markovian Dynamics of Open Quantum Systems*, Phys. Rev. Lett. **109**, 170402 (2012).
- [43] M. M. Ali, P.-Y. Lo, M. W.-Y. Tu, and W.-M. Zhang, *Non-Markovianity measure using two-time correlation functions*, Phys. Rev. A **92**, 062306 (2015).
- [44] I. d. Vega and D. Alonso, *Dynamics of non-Markovian open quantum systems*, Rev. Mod. Phys. **89**, 015001 (2017).
- [45] W.-M. Zhang, *Exact master equation and general non-Markovian dynamics in open quantum systems*, Eur. Phys. J. Special Topics, **227**, 1849 (2019).
- [46] A. L. Leggett, S. Chakravarty, A. T. Dorsey, M. P. A. Fisher, A. Garg, and W. Zwerger, *Dynamics of the dissipative two-state system*, Rev. Mod. Phys. **59**, 1 (1987).
- [47] N. S. Wingreen, A.-P. Jauho, and Y. Meir, *Time-dependent transport through a mesoscopic structure*, Phys. Rev. B **48**, 8487(R) (1993).
- [48] A.-P. Jauho, N. S. Wingreen, and Y. Meir, *Time-dependent transport in interacting and noninteracting resonant-tunneling systems*, Phys. Rev. B **50**, 5528 (1994).
- [49] R. Tsu, L. Esaki, *Tunneling in a finite superlattice*, Appl. Phys. Lett. **22**, 562-564 (1973).
- [50] L. L. Chang, L. Esaki, R. Tsu, *Resonant tunneling in semiconductor double barriers*, Appl. Phys. Lett. **24**, 593 (1974).
- [51] T. C. L. G. Sollner, W. D. Goodhue, P. E. Tannenwald, C. D. Parker, D. D. Peck, and H. Q. Le, *Resonant tunneling through quantum wells at frequencies up to 2.5 THz*, Appl. Phys. Lett. **43**, 588 (1983).
- [52] S. Luryi, *Frequency limit of double-barrier resonant-tunneling oscillators*, Appl. Phys. Lett. **47**, 490 (1985).
- [53] F. Capasso, K. Mohammed and A. Cho, *Resonant tunneling through double barriers, perpendicular quantum transport phenomena in superlattices, and their device applications*, IEEE J. Quant. Electron, **22**, 1853 (1986).
- [54] H. B. Heersche, Z. de Groot, J. A. Folk, H. S. J. van der Zant, C. Romeike, M. R. Wegewijs, L. Zobbi, D. Barreca, E. Tondello, and A. Cornia *Electron Transport through Single Mn12 Molecular Magnets*, Phys. Rev. Lett. **96**, 206801 (2006).
- [55] X. W. Tu, G. Mikaelian, and W. Ho, *Controlling Single-Molecule Negative Differential Resistance in a Double-Barrier Tunnel Junction*, Phys. Rev. Lett. **100**, 126807 (2008).
- [56] M. Perrin, R. Frisenda, M. Koole et al., *Large negative differential conductance in single-molecule break junctions*, Nat. Nanotechnol. **9**, 830 (2014).
- [57] T. Kwapiński, R. Taranko, *Time-dependent transport through a quantum dot with the over-dot (bridge) additional tunneling channel*, Physica E Low Dimens. Syst. Nanostruct., **18**, 402 (2003).
- [58] B. Dong, G. H. Ding and X. L. Lei, *Time-dependent quantum transport through an interacting quantum dot beyond sequential tunneling: second-order quantum rate equations*, J. Phys. Condens. Matter **27**, 205303 (2015).
- [59] L. Chua, *Memristor-The missing circuit element*, IEEE Trans. Circuit Theory **18**, 507 (1971).
- [60] M. Itoh, and L. O. Chua, *Memristor oscillators*, IJBC, **18**, 3183 (2008).
- [61] D. B. Strukov, G. S. Snider, D. R. Stewart, and R. S. Williams, *The missing memristor found*, Nature, **453**, 80 (2008).
- [62] I. Abraham, *The case for rejecting the memristor as a fundamental circuit element*, Sci. Rep. **8**, 10972 (2018).
- [63] B. Tellini, M. Bologna, K. J. Chandía, M. Macucci, *Revisiting the memristor concept within basic circuit theory*, Int. J. Circuit Theory Appl., **49**, 3488 (2021).
- [64] D. A. Doyle, J. Morais Cabral, R. A. Pfuetzner, A. Kuo, J. M. Gulbis, S. L. Cohen, B. T. Chait, and R. MacKinnon, *The Structure of the Potassium Channel: Molecular Basis of K+ Conduction and Selectivity*, Science **208**, 69 (1998).
- [65] Q. Wang, Y. F. Chen, S. B. Long, J. B. Niu, C. S. Wang, R. Jia, B. Q. Chen, M. Liu, T. C. Ye, *Fabrication and characterization of single electron transistor on SOI*, Microelectron. Eng. **84**, 1647 (2007).
- [66] P. S. Boggio, R. Ferrucci, S. P. Rigonatti, P. Covre, M. Nitsche, A. Pascual-Leone, F. Fregni, *Effects of transcranial direct current stimulation on working memory in patients with Parkinson's disease*, J. Neurol. Sci. **249**, 31 (2006).
- [67] J. Holmes, S. E. Gathercole, and D. L. Dunning, *Adaptive training leads to sustained enhancement of poor working memory in children*, Dev. Sci. **12**, F9 (2009).
- [68] S. C. Andrews, K. E. Hoy, P. G. Enticott, Z. J. Daskalakis, P. B. Fitzgerald, *Improving working memory: the effect of combining cognitive activity and anodal transcranial direct current stimulation to the left dorsolateral prefrontal cortex*, Brain Stimul. **4**, 84 (2011).
- [69] A. R. Brunoni, M.-A. Vanderhasselt, *Working memory improvement with non-invasive brain stimulation of the dorsolateral prefrontal cortex: A systematic review and meta-analysis*, Brain Cogn. **86**, 1 (2014).
- [70] E. Neher and B. Sakmann, *Single-channel currents recorded from membrane of denervated frog muscle fibres*,

- Nature **260**, 799 (1976).
- [71] B. Sakmann and E. Neher, *Single Na⁺ channel currents observed in cultured rat muscle cells*, Nature **287**, 447 (1980)
- [72] N. Fertig, M. Klau, M. George, R. H. Blick, and J. C. Behrends, *Activity of single ion channel proteins detected with a planar microstructure*, Appl. Phys. Lett. **81**, 4865 (2002).
- [73] J. Shuai, and I. Parker, *Optical single-channel recording by imaging Ca²⁺ flux through individual ion channels: theoretical considerations and limits to resolution*, Cell calcium **37**, 283 (2005).
- [74] M. Mortensen, and T. G. Smart, *Single-channel recording of ligand-gated ion channels*, Nat. Protoc. **2**, 2826 (2007).
- [75] J. K. Rosenstein, S. Ramakrishnan, J. Roseman, and K. L. Shepard, *Single ion channel recordings with CMOS-anchored lipid membranes*, Nano Lett. **13**, 2682 (2013).
- [76] H. Tsukamoto, Y. Furutani, in *Optogenetics, Optogenetic Modulation of Ion Channels by Photoreceptive Proteins*, edited by H. Yawo, H. Kandori, A. Koizumi, and R. Kageyama (Springer, Singapore, 2021)
- [77] E. G. Govorunova, Y. Gou, O. A. Sineshchekov, H. Li, X. Lu, Y. Wang, L. S. Brown, F. St-Pierre, M. Xue, and J. L. Spudich, *Kalium channelrhodopsins are natural light-gated potassium channels that mediate optogenetic inhibition*, Nat. Neurosci. **25**, 967 (2022).
- [78] S. M. Sternson, and B. L. Roth, *Chemogenetic Tools to Interrogate Brain Functions*, Annu. Rev. Neurosci. **37**, 387 (2014).
- [79] B. L. Roth, *DREADDs for Neuroscientists*, Neuron **89**, 683 (2016).
- [80] E. J. Campbell, N. J. Marchant, *The use of chemogenetics in behavioural neuroscience: receptor variants*, Br. J. Pharmacol. **175**, 994 (2018).